# Electrochemical and Morphological Characterization of New Architectures Containing Self-Assembled Monolayers and Au-NPs

**Virgínia C. Ferreira,[†,‡] A. Fernando Silva,[‡] and Luisa M. Abrantes[†,*]**

*CQB, Departamento de Química e Bioquímica, Faculdade de Ciências da Universidade de Lisboa, Campo Grande, 1749-016 Lisboa and CIQ-UP, Linha 4, Departamento de Química, Faculdade de Ciências da Universidade do Porto, Rua do Campo Alegre 687, 4169-007 Porto, Portugal*

*Received: December 23, 2009; Revised Manuscript Received: February 12, 2010*

Pure 1,10-decanedithiol ($C_{10}$-SH) and mixed (1-decanethiol:1,10-decanedithiol) self-assembled monolayers (SAMs) prepared from ethanolic solution on Au(111) surfaces have been used in order to investigate the effect of the SAM organization and the availability of free −SH groups at the SAM/solution interface on the development of layer-by-layer architectures containing SAMs and gold nanoparticles (Au-NPs). The SAM modified electrodes have been electrochemically characterized by cyclic voltammetry in alkaline medium (reductive desorption) and in the presence of an electroactive species, $Fe(CN)_6^{3-}$, in $KNO_3$ solution, enabling the evaluation of the stability and organization of the SAMs. Enhanced stability, organization, and hindrance to the electron transfer were found for the mixed SAMs with increasing thiol content, when compared with the pure dithiol SAM. The mixed SAM prepared from solution containing the thiol to dithiol proportion of (50:1) and pure $C_{10}$-SH SAMs have been selected for further modification; the electrochemical quartz crystal microbalance (EQCM) enables the detection of different amount of citrate stabilized Au-NPs attachment to the selected SAMs modified electrodes due to distinct availability of free −SH groups at the SAM/solution interface and the electrochemical characterization of the layer-by-layer assemblies (based on pure $C_{10}$-SH and mixed SAMs) showed that the electron transfer (ET) properties of the such architectures strongly depend on the nature of the base SAM and amount of immobilized Au-NPs. Atomic force microscopy (AFM) morphological characterization of the $C_{10}$-SH SAM upon layer-by-layer modification was performed ex situ in air.



## Introduction

Self-assembled monolayers (SAMs) have been widely used in the past decades due to their ease of preparation, organization, and versatility.[1,2] The self-assembling process enables the possibility of tuning the surface properties by simple modification of the adsorbed molecules characteristics, namely chain length, conjugated/insulating properties, and terminal functional group. On gold surfaces, the strong interaction between sulfur and gold is the driving force for self-assembling of sulfur-containing molecules, such as thiols and disulfides, and justifies the extensive use of this type of compounds.[1,2] Investigation has been devoted to α,ω-dithiol SAMs (aliphatic or aromatic) since these molecules, presenting two −SH functionalities, allow the surface modification displaying free −SH groups at the SAM/solution (or air) interface.[3] However, some difficulties have arisen from the self-assembling process of dithiol compounds due to the possibility of loops formation (both −SH functionalities binding to the gold surface) and consequent loss of organization and compactness;[4] the possibility of inter- and intralayer disulfide bonding has also been considered for this lack of organization.[5–12] In this case, the presence of oxidizing species in the self-assembling solution, such as oxygen, which is a highly interfering component, may contribute to the oxidation of the −SH terminal groups at the SAM/solution interface.[13] It has been reported in the literature that, depending on the self-assembling conditions (adsorbate properties, concentration, solvent, and temperature), the dithiol molecules can adopt different configurations, parallel to the surface, looped or with an upright orientation.[4,13–18] However, these modified surfaces, allowing the attachment to other functionalities such as metallic ions,[19,20] metals (e.g., by vacuum deposition or electrochemical reduction of metallic ions in solution),[3,9,21–24] and presynthesized gold nanoparticles,[15–18,25,26] reinforce the possibility of a single −SH group attachment to the gold surface.

Some approaches have been used envisaging the formation of more compact and organized SAMs displaying free −SH groups at the SAM/solution interface and for the control over the SAM composition and nanopatterning.[3,27] A promising one-step procedure is the simultaneous coadsorption of alkanethiol and alkanedithiol molecules, in which advantage is taken from the stability and organization conferred by the van der Waals interactions between alkyl chains of the alkanethiol component, which increases with the chain length,[28,29] facilitating the attachment of dithiol molecules through a single −SH group to the gold surface.[27]

Thiol-functionalized SAMs have been applied for the development of 2D and 3D architectures with gold nanoparticles (Au-NPs). Distinct routes have been used: Au-NPs surface modification with dithiol molecules, in solution, and immobilization on gold electrodes,[16,30,31] attachment of Au-NPs on dithiol SAMs through Au−S bonding,[15,17,18,26] and multilayer formation by alternate immersion in dithiol solution and colloidal suspension.[16,25,32,33]

* To whom correspondence should be addressed. Phone: +351 21 7500890. Fax: +351 21 7500088. E-mail: luisa.abrantes@fc.ul.pt.
† CQB, FCUL, Universidade de Lisboa.
‡ Present address: CIQ-UP, Linha 4, FCUP, Universidade do Porto.

10.1021/jp912123m 
Published on Web 04/13/2010

It is well-known that long-chain alkanethiol SAMs act as insulating barriers, with the electron transfer at compact and organized SAMs modified electrodes being strongly hampered.[34] Compact and organized α,ω-alkanedithiol SAMs, free of defected and collapsed sites at which the ET easily occurs,[25,26] can act as insulating barriers as efficiently as alkanethiol SAMs.[13,15,17,18,26,30]

Upon Au-NPs immobilization, it has been reported that the ET between an electroactive species in solution and the electrode surface is facilitated[17,18,25,26] depending, namely, on the compactness and organization of the SAM and the distribution and distance of the Au-NPs to the electrode surface. Brust and coworkers investigated the effect of α,ω-alkanedithiol and Au-NPs multilayers and found that for the dithiol exposed layer, the ET is suppressed, and as a new layer of Au-NPs is immobilized, a quasi-reversible voltammetric profile is restored with peak separation increasing with the number of Au-NPs layers.[16,32] These authors suggest that the ET can occur between Au-NPs through the layers but the heterogeneous ET can only occur at the exposed Au-NPs surface. On the other hand, in an similar system, Lu et al. verified that for 1,6-hexanedithiol and citrate/Au-NPs multilayers, with the increasing number of layers, the ET is more strongly hampered for the interface dithiol/electrolyte, whereas an enhanced reversibility was detected when the Au-NPs were exposed to the solution.[25]

Joseph et al. have shown that in an analogous layer-by-layer assembling process, the conductance increases with the number of Au-NPs layers.[33] For these multilayer systems it was found that the cross-linking of Au-NPs with dithiol molecules enhances the conductivity of the modified electrode, namely, when compared with alkanethiol protected nanoparticles systems.

In the present contribution, 1,10-decanedithiol and mixed (1,10-decanedithiol and 1-decanethiol) SAMs have been electrochemically characterized envisaging its further use as platforms for the attachment of citrate-stabilized Au-NPs and SAMs/Au-NPs architectures development. Electrochemical quartz crystal microbalance and atomic force microscopy have been used to monitor the Au-NPs immobilization (in the first layer) and morphological evolution of the multilayer system, respectively, and the electron transfer properties of the modified electrodes, accessed by cyclic voltammetry.

## Experimental Section

Gold-coated slides (1.1 × 1.1 $cm^2$, Gold Arrandee, Germany) were used; the surfaces were cleaned with piranha solution (3:1 mixture (v/v) of $H_2SO_4$ (Fluka, 95−97%) and $H_2O_2$ 30% (Fluka, p.a.)), rinsed with copious amounts of ultrapure water and ethanol, and flame annealed, leading to a predominantly (111) crystallographic orientation and a surface roughness $R = 1.2$.

Pure SAMs were prepared by immersion (22 h) of the clean gold surfaces in ethanolic solutions (Panreac, ≥ 99.9%), previously deaerated with $N_2$ (90 min), containing 1 mM 1,10-decanedithiol ($C_{10}$-SH) (AlphaAesar, purity ≥95%) or 1-decanethiol ($C_{10}$) (AlphaAesar, purity ≥96%), which will be referred to as pure dithiol and thiol SAMs, respectively. Mixed SAMs were obtained from solutions containing $C_{10}$ and $C_{10}$-SH (22 h) with concentration ratios of (5:1), (10:1), or (50:1) and a final concentration of 1 mM. After the adsorption period, the modified gold surfaces were copiously rinsed with ethanol and water and dried under a nitrogen flow.

Gold clusters of 15 nm average diameter were synthesized by the Turkevich method[35,36] through citrate reduction in aqueous medium at about 100 °C. Briefly, to a 5.0 μmol of $HAuCl_4$ (AlfaAesar, 99.99%) in 19 mL of $H_2O$ boiling solution, vigorously stirred, was added rapidly 2 mL of 0.5% sodium citrate dihydrate (AlfaAesar, 99.0%) solution, resulting in a color change from pale yellow to reddish in a few seconds. Boiling and stirring was continued for ca. 5 min; the heating was then turned off. The colloidal solution was stirred for an additional 30 min. After the solution reached room temperature it was stored in the dark at 4 °C. The gold nanoparticles synthesized by this procedure are stabilized by a layer of citrate anions adsorbed on their surface and will be referred to as citrate/Au-NPs. The so obtained gold nanoparticles colloidal suspensions were characterized by UV−visible spectrophotometry (UV−vis, Jasco V560 spectrophotometer), Transmission Electron Microscopy (TEM, Hitachi H-8100 transmission electron microscope, operating at 15 kV), and X-ray diffraction (XRD, Philips - PW 1710 diffractometer with Cu Kα radiation ($\lambda = 1.5418$ Å) operated at 40 kV and 20 mA with a time per step of 5.000 s and a step size of 0.010°). The morphological characterization of SAMs and Au-NPs modified electrodes was performed by atomic force microscopy (AFM) ex situ, in air, tapping mode, at an Atomic Force Microscope (Nanoscope IIIa Multimode-Digital Instruments).

The citrate-stabilized gold nanoparticles were immobilized onto the dithiol or mixed SAMs by immersion of the modified electrodes in the colloidal suspension for ca. 22 h. Following the immobilization, the electrodes were thoroughly washed with ultrapure water, in order to remove any physically adsorbed particles, and dried under a nitrogen flow, before characterization or transfer to the 1,10-decanedithiol solution (for the dithiol and Au-NPs layer-by-layer assembly).

Electrochemical experiments were performed with an IMT Electrochemical Interface and a DEA332 Digital Electrochemical Analyzer connected to a computer for data acquisition (VoltaMaster2 software). A one-compartment cell, with the gold-coated glass as working electrodes (0.57 $cm^2$ exposed geometrical area), a Pt wire counter-electrode, and a saturated calomel reference electrode (SCE), were used.

The SAMs were electrochemically characterized by reductive desorption (by means of potential cycling at $\nu = 20$ mV $s^{-1}$ between 0 and −1.25 V) in 0.1 M NaOH solution (Panreac, p.a.). The sample-to-sample variability in the peaks position is ±10 mV. Electrochemical characterization of the SAM or SAM/Au-NPs modified electrodes, in the presence of the redox probe $K_3Fe(CN)_6$ (1 mM in $KNO_3$ 0.1 M, pH 7), was performed between −0.3 and 0.65 V at $\nu = 50$ mV $s^{-1}$.

The electrochemical quartz crystal microbalance (EQCM) experiments were performed with a frequency analyzer (CH Instruments model 420, sensitivity 7 μg $kHz^{-1}$), in a single compartment cell. The working electrode was an 8 MHz AT-cut quartz crystal coated with 100 Å Ti and 1000 Å Au (0.2 $cm^2$ exposed geometrical area).

Prior to all measurements, the solutions, prepared with ultrapure water, were degassed with $N_2$ (99,9999%) for 15 min (or 1 h in the case of NaOH solution).

## Results and Discussion

**Gold Nanoparticles Characterization.** The synthesized spherical citrate-stabilized gold nanoparticles present a strong plasmon resonance absorption band at about 522 nm, as illustrated in the UV−visible spectra in Figure 1a, which is in agreement with the values usually reported for small sized particles of ca. 14−20 nm.[37−39] The size of the spherical citrate/Au-NPs has been confirmed by TEM analysis, as depicted in the representative image in Figure 1b. The size distribution

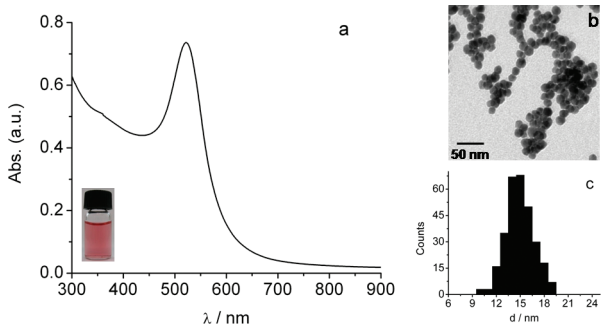


**Figure 1.** (a) UV−vis spectra and digital photograph (inset) of the colloidal gold suspension, (b) representative TEM image, and (c) size distribution histogram of the synthesized gold nanoparticles.

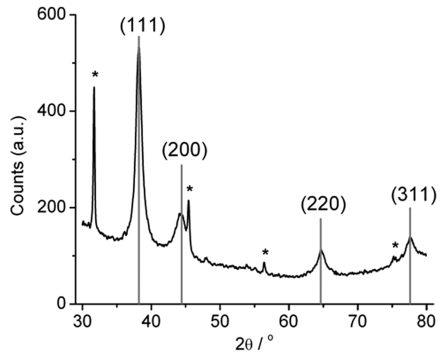


**Figure 2.** XRD pattern of the spherical gold nanoparticles deposited on silicon.

histogram, Figure 1c, shows the diameter of the particles of about 15.1 ± 1.8 nm.

Figure 2 shows the XRD pattern of the citrate/Au-NPs deposited on an amorphous silicon slide. The diffraction peaks at 38.14°, 44.30°, 64.64°, and 77.62° correspond to the (111), (200), (220), and (311) facets, respectively, demonstrating that the deposited gold particles are composed of pure crystalline gold with the face-centered cubic structure (JCPDS file No. 4-0784). The relative intensities ($I/I_{111}$) of the peaks (1.00, 0.22, 0.15, and 0.13) indicate that the nanoparticles structure has a tendency to grow with the surfaces dominated by the lowest energy (111) facets, since lower values than those of the standard file of gold (1.00, 0.52, 0.32, and 0.36) were obtained.

Additional diffraction peaks, identified in the figure with an asterisk, occurring at $2\theta$ values of 31.69°, 45.45°, 56.48°, and 75.30°, have been investigated and can be assigned to NaCl peaks (JCPDS file No. 5-0628), since both $Na^+$ and $Cl^-$ are present in the synthesis medium from sodium citrate and $HAuCl_4$, respectively.

**Electrochemical Characterization of 1,10-Decanedithiol and Mixed SAMs Modified Electrodes.** In this work, 1,10-decanedithiol ($C_{10}$-SH) and mixed (1-decanethiol ($C_{10}$) and 1,10-decanedithiol) self-assembled monolayers, prepared from solution, have been investigated in order to obtain Au(111) modified electrodes displaying appropriate electrochemical properties and incorporating specific functionalities for the development of architectures involving SAMs and Au-NPs. Those molecules adopt a hexagonal $(\sqrt{3}\times\sqrt{3})R30°$ structure commensurate with the underlying gold surface, as evidenced by STM studies.[5,11,40] The analysis of the reductive desorption profiles of the pure SAMs prepared from 1-decanethiol and 1,10-decanedithiol have been previously reported.[5]

In Figure 3 are shown the cyclic voltammograms of the reductive desorption of mixed monolayers formed from ethanolic solutions containing different thiol to dithiol proportions ((5:1), (10:1), and (50:1)), from which the data presented in Table 1 was collected. From the voltammetric profiles, it can be observed that the presence of $C_{10}$ in the mixed monolayers increases the SAMs stability and the reductive desorption peak, $E_{p1}$, occurs at potential values more negative than that of the pure $C_{10}$-SH SAM ($E_{p1} = -1018$ and $E_{p2} = -1170$ mV);[5] the second reductive desorption peak potential, $E_{p2}$, is basically independent of the SAM composition. The surface coverage values, Table 1, show that enhanced organization can be achieved from the formation of mixed SAMs from solutions containing a high proportion of thiol (50:1). In this case, Γ values of the same order of that estimated for a compact and organized alkanethiol monolayer on Au(111) ($\Gamma_{theo.} = 7.6 \times 10^{-10}$ mol $cm^{-2}$)[28,29] indicate that the dithiol molecules are likely to adopt an upright orientation rather than spreading flat on the surface and bound through their −SH groups to form dithiol bounded domains. Therefore, the presence of the $C_{10}$ in the mixed SAM seems to improve its organization ($E_p$ comparable to that of the $C_{10}$ SAM[5] and a higher Γ than for the other mixed SAMs), which is an important issue for the availability and adequate positioning of the −SH functional groups at the SAM/solution interface for further surface modification.

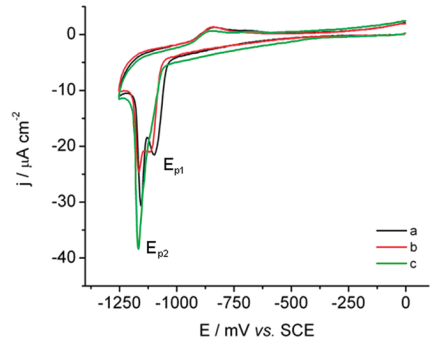


**Figure 3.** Voltammetric profiles of the reductive desorption of the mixed SAMs prepared with the ($C_{10}$:$C_{10}$-SH) proportions of (a) (5:1), (b) (10:1), and (c) (50:1) prepared with $t_{ads} = 22$ h; NaOH 0.1 M at $\nu = 20$ mV $s^{-1}$.

The results revealed that advantage has been taken from the formation of mixed SAMs, namely, the SAM disorganization (due to the existence of two thiol functionalities in the 1,10-decanedithiol molecules) has been overcome by the stability conferred by the presence of the long alkyl chain 1-decanethiol.

The final composition of the mixed SAMs depends on several factors, namely the properties of the components such as solubility, chain length, and terminal group, the molar ratio, concentration, and solvent used.[3,27,41] Moreover, it has been reported in the literature that the composition of the mixed SAM, prepared from a solution containing both 1-octanethiol and 1,8-octanedithiol, does not reflect the solution concentration ratio, namely for a proportion of (199:1) thiol/dithiol, the SAM composition was (2:1) thiol/dithiol,[27] probably due to the presence of two −SH functionalities in the dithiol molecule, the possibility of these molecules binding to the surface is higher than that of the thiol.

Since both $C_{10}$ and $C_{10}$-SH SAMs reductive desorption occurs in the same potential range, especially the reductive desorption peak at more negative values, $E_{p2}$, it has not been possible to infer on the final composition of the mixed SAMs. Barely the relative intensity of this second reductive desorption peak, intensified with the $C_{10}$ content in the preparation solution, may suggest the prevalence of this component within the (50:1) mixed SAM, given that the same trend was detected for pure $C_{10}$ SAM.

**TABLE 1: Potential of the reductive desorption peaks ($E_p$) and surface coverage ($\Gamma$) values of the SAMs**

| SAM | $t_{ads}$/h | $E_{p1}$/mV | $E_{p2}$/mV | $\Delta E_p$[a]/mV | $10^{10}\Gamma_{RQ}$ (±0.1)/mol cm$^{-2}$ |
|---|---|---|---|---|---|
| $C_{10}$ 1 mM | 22 | −1100 | −1165 | 65 | 7.4[b] |
| $C_{10}$-SH 1 mM | | −1018 | −1170 | 152 | 6.2[b] |
| $C_{10}$:$C_{10}$-SH (5:1) | | −1098 | −1155 | 57 | 6.3 |
| $C_{10}$:$C_{10}$-SH (10:1) | | −1123 | −1166 | 43 | 6.2 |
| $C_{10}$:$C_{10}$-SH (50:1) | | ca. −1109[c] | −1167 | ∼58 | 7.1 |

[a] Reductive desorption peaks separation. [b] From ref 5. [c] Shoulder.

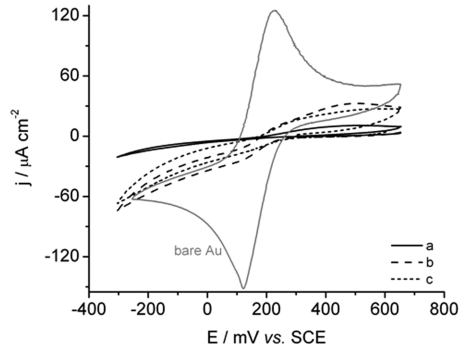


**Figure 4.** Cyclic voltammograms of the pure SAMs characterization [(a) $C_{10}$ ($t$ = 22 h), (b) $C_{10}$-SH ($t$ = 22 h), and (c) $C_{10}$-SH ($t$ = 40 h)] and comparison with (—) bare Au, in 1 mM $K_3Fe(CN)_6$ in 0.1 M $KNO_3$ solution; $\nu$ = 50 mV s$^{-1}$.

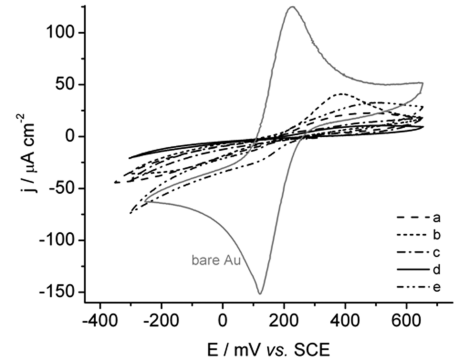


**Figure 5.** Cyclic voltammograms of the characterization of mixed SAMs, prepared with $t$ = 22 h [(a) $C_{10}$:$C_{10}$-SH (5:1), (b) $C_{10}$:$C_{10}$-SH (10:1), and (c) $C_{10}$:$C_{10}$-SH (50:1)] and comparison with pure SAMs ($t$ = 22 h) [(d) $C_{10}$, (e) $C_{10}$-SH] and (—) bare Au, in 1 mM $K_3Fe(CN)_6$ in 0.1 M $KNO_3$ solution; $\nu$ = 50 mV s$^{-1}$.

To achieve a better insight into the barrier properties and compactness of the studied monolayers, those have been characterized by cyclic voltammetry in $KNO_3$ solution containing 1 mM $Fe(CN)_6^{3-}$. In Figures 4 and 5 are depicted the voltammetric profiles obtained for the pure and mixed SAMs, respectively. It can be observed that, while in the $C_{10}$ modified electrode the electron transfer is strongly hampered, lower hindrance (of the ET) is detected for the $C_{10}$-SH SAM. In fact, compact and organized alkanethiol SAMs are known to act as insulating barriers to the electron transfer between an electroactive species in solution and the electrode surface.[34] On the other hand, the sigmoidal shape of the voltammogram obtained for the dithiol SAM suggests the presence of defects and collapsed sites within the monolayer,[13,34] probably due to the formation of loops and consequently a less-ordered $C_{10}$-SH SAM,[5] as has also been indicated by the electrochemical data discussed above. In this case, the increase in the adsorption time ($t$ = 40 h) does not seem to significantly improve this SAM organization.

For the mixed SAMs, it was found that the presence of $C_{10}$ in the $C_{10}$-SH monolayer decreases SAM defects and enhances its organization, possibly by preventing loops formation,[3,5,27] since higher hindrance to the ET was detected in Figure 5. Although similar voltammetric profiles have been observed in the cathodic scan for the (5:1) and (10:1) mixed SAMs, the increase from (10:1) to (50:1) of the $C_{10}$ content in the preparation solution has clearly improved the barrier properties of the later SAM and thus its organization, as has also been pointed out by the electrochemical information obtained from reductive desorption studies.

**Self-Assembled Heterostructures Containing SAMs and Citrate/Au-NPs.** From the electrochemical results presented above, 1,10-decanedithiol and mixed (50:1) SAMs, bearing free −SH groups adequate for Au-NPs immobilization, have been selected for the construction of architectures involving SAMs and citrate/Au-NPs. As the layer-by-layer structures are built on the Au(111) surface, by alternate immersion in $C_{10}$-SH 1 mM ethanolic solution and citrate/Au-NPs suspension, the surface morphology is altered as can be detected in the AFM images presented in Figure 6. The $C_{10}$-SH SAM presents a smooth surface and atomic steps of the underlying gold surface can be clearly identified, Figure 6a. Upon citrate/Au-NPs immobilization significant changes are observed in the surface. Spherical shaped features with an average diameter of 11.1 nm appear in the topographic image in Figure 6b, which are close to the Au-NPs diameter of about 15 nm and the rms roughness, Rq, increases from 0.31 nm, in the $C_{10}$-SH SAM, to 0.55 nm. Dissimilarly to the $C_{10}$-SH SAM layer, Figure 6a′, enhanced phase contrast is detected in Figure 6b′, due to distinct viscoelastic properties of the SAM and Au-NPs on the surface. As a new immersion step in $C_{10}$-SH solution is performed, a new layer of dithiol is formed on the Au-NPs surface as suggested by the Rq decrease to 0.35 nm and the enlarged diameter of the spherical features ($\phi$ = 13.5 nm), probably due to the effect of the SAM adsorbed on the Au-NPs surface, Figure 6c, which is corroborated by the phase image in Figure 6c′ revealing the re-emergence of a homogeneous layer.

The citrate/Au-NPs immobilization on the first layer modified electrodes has been monitored by EQCM. Following an initial period of stabilization of the SAM in ultrapure water, the colloidal suspension is added to the cell compartment and the attachment takes place. In Figure 7 are illustrated the frequency changes during the immobilization process in pure $C_{10}$ and $C_{10}$-SH and mixed (50:1) monolayers (prepared from 1 mM solutions and $t$ = 22 h).

Assuming a rigid layer behavior of the SAM and therefore using the Sauerbrey equation,[42] the amount of citrate/Au-NPs immobilized on the modified surfaces has been estimated from the changes in the resonant frequency of the EQCM, $\Delta f$, Table 2. The volume of the unitary cell of Au (fcc) was 0.054 nm$^3$. The calculated mass of the citrate/Au-NPs, $m_{Au\text{-}NPs}$, with average size of 15.1 nm (stabilized by a monolayer of citrate ions adsorbed on the nanoparticles surface) was 0.027 g nmol$^{-1}$. The surface coverage, of Au-NPs on the SAM, D, after $t_{immob.}$= 800 s, was obtained from the mass change, $\Delta m$, and $m_{Au\text{-}NPs}$. Taking into account that Au-NPs can also be physically

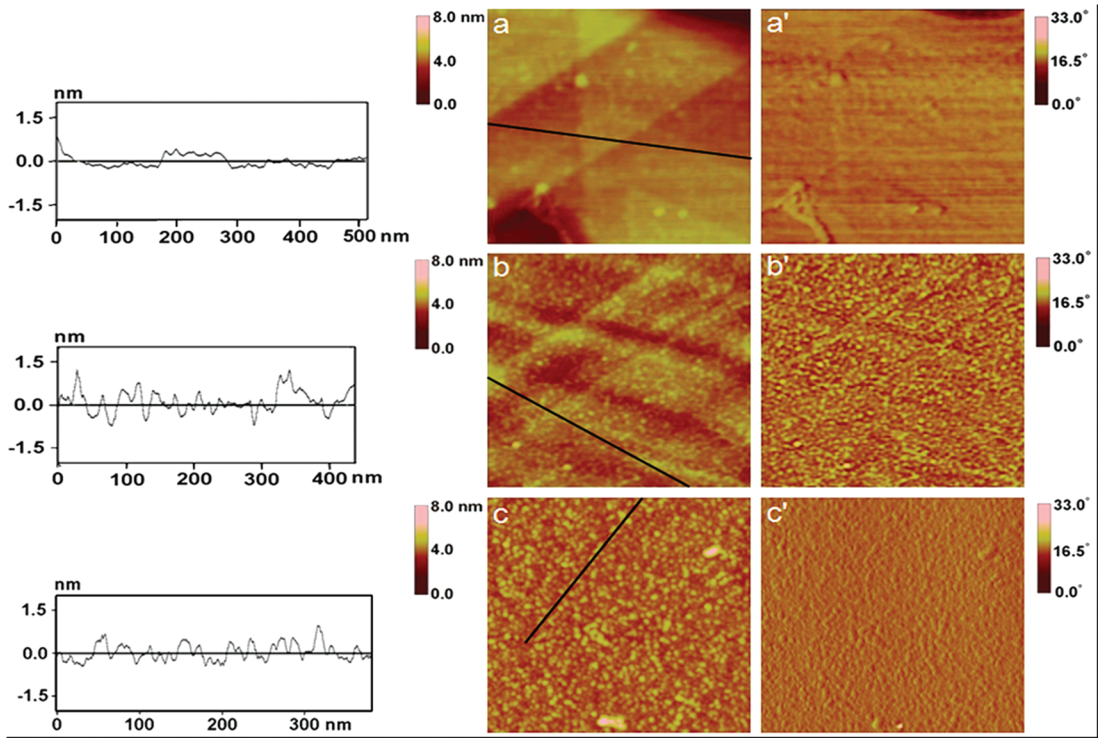


**Figure 6.** Tapping mode AFM images, topographic and profile (a−c) and phase (a′−c′), of the Au(111) modified electrodes with (a) $C_{10}$-SH SAM, (b) $C_{10}$-SH/Au-NPs, and (c) $C_{10}$-SH/Au-NPs/$C_{10}$-SH. (500 × 500) nm$^2$ AFM images; topography: $z$ = 8 nm and phase $z$ = 33°.

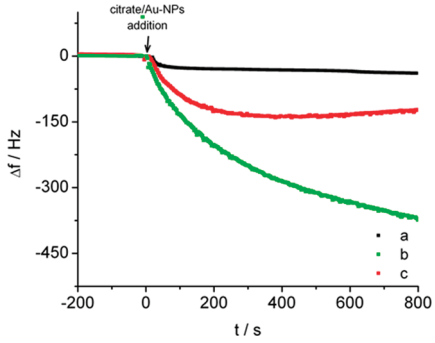


**Figure 7.** Resonant frequency change in the quartz crystal microbalance during the citrate/Au-NPs immobilization on SAM ($t$ = 22 h) modified gold electrodes: (a) $C_{10}$, (b) $C_{10}$-SH, and (c) (50:1) mixed monolayers.

immobilized on the SAMs, a control experiment has been performed on 1-decanethiol modified electrode that presents methyl terminal groups at the SAM/solution interface and no specific interaction should occur between this SAM and the Au-NPs. As expected, the frequency change observed for this SAM ($\Delta f$ = −39.33 Hz) is lower than that registered for the −SH functionalized monolayers, as depicted in Table 2, and the mass associated with nonspecific interactions has been subtracted for calculations purpose.

The maximum surface coverage of 15.1 nm citrate/Au-NPs, in a close packed arrangement, on a dithiol SAM would be $D_{max.}$ = 5.6 × 10$^{11}$ parts·cm$^{-2}$. The estimated submonolayer amount of Au-NPs immobilized on the $C_{10}$-SH and mixed (50:1) SAMs, through Au−S bonding, $D'$, was 9.2% and 3.4% of $D_{max.}$, respectively, which may be due to repulsive interactions between the negatively charged citrate-stabilized Au-NPs[15] and the lack of appropriate orientation of the free −SH groups on the SAM/solution interface. It is worth mentioning that, after the immobilization time of 800 s, the amount of citrate/Au-NPs attached to the $C_{10}$-SH SAM has not attained its maximum value, suggesting that the number of nanoparticles immobilized on this SAM will be higher when the modification time, used in this work ($t$ = 22 h), is accomplished. The balance between the electrostatic repulsions (negatively charged Au-NPs) and strong Au−S interaction (Au-NPs attachment to free −SH groups at the SAM/solution interface) may be the driving forces controlling the time scale of the assembling process, larger than at −$CH_3$ functionalized $C_{10}$ SAM (physical interaction) and at mixed SAM with diluted −SH functions in a −$CH_3$ terminal SAM.

The obtained results clearly show that depending on the SAM composition different amounts of nanoparticles can be attached to the surface through Au−S bonding and that the formation of mixed SAMs may enable the control over the amount and possibly the distribution of the Au-NPs on the SAM modified surface.

The layer-by-layer architectures of SAMs and citrate/Au-NPs studied here have been electrochemically characterized in $KNO_3$ solution containing 1 mM $Fe(CN)_6^{3-}$. In this case, two distinct Au(111) modified electrodes (first layer) have been investigated, the $C_{10}$-SH and the (50:1) mixed SAMs (prepared with $t$ = 22 h) since, as has been shown by the EQCM data, pure dithiol and the selected mixed SAM enable the attachment of different amounts of Au-NPs. Figures 8 and 9 illustrate the cyclic voltammograms obtained for the consecutive layers based on the $C_{10}$-SH and (50:1) mixed SAM modified electrodes, respectively.

The results show that upon Au-NPs immobilization, in both $C_{10}$-SH and mixed SAM modified electrodes, an increase in the ET occurs, suggesting the improvement of the electron transfer process between the electroactive species in solution and the electrode surface due to the presence of the nanoparticles. The observed behavior is in agreement with the investigations reported in the literature, were the impediment to the ET in alkanedithiol and citrate/Au-NPs modified electrodes, using the same redox probe, decreased with the immobilization of the

**TABLE 2: Resonant Frequency Change ($\Delta f$), Calculated Mass ($\Delta m$), and Estimated Amount of Immobilized Citrate/Au-NPs on the SAMs ($D$)**

| SAM | $t_{immob}$/s | $\Delta f$/Hz | $\Delta m/\mu g\ cm^{-2}$ | $D$/parts·cm$^{-2}$ | $D'$ [a]/parts·cm$^{-2}$ |
|---|---|---|---|---|---|
| $C_{10}$ | 800 | −39.33 | 0.27 | $0.61 \times 10^{10}$ | |
| $C_{10}$-SH | | −374.22 | 2.59 | $5.79 \times 10^{10}$ | $5.18 \times 10^{10}$ |
| $C_{10}$:$C_{10}$-SH (50:1) | | −121.98 | 0.84 | $1.89 \times 10^{10}$ | $1.28 \times 10^{10}$ |

[a] Surface coverage of citrate/Au-NPs immobilized on the SAM through Au−S bonding.

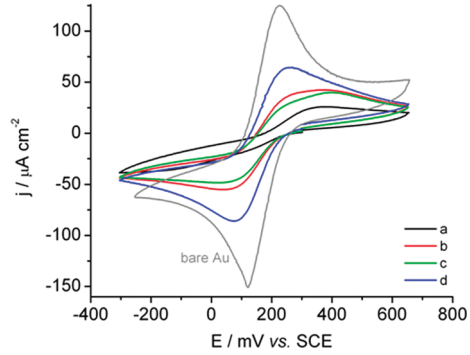


**Figure 8.** Voltammetric profiles of the Au(111) modified electrodes with (a) $C_{10}$-SH SAM, (b) $C_{10}$-SH/Au-NPs, (c) $C_{10}$-SH/Au-NPs/$C_{10}$-SH, and (d) $C_{10}$-SH/Au-NPs/$C_{10}$-SH/Au-NPs, in 1 mM $K_3Fe(CN)_6$ in 0.1 M $KNO_3$ solution; $\nu = 50$ mV s$^{-1}$.

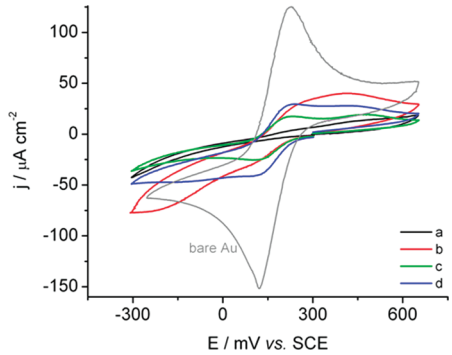


**Figure 9.** Voltammetric profiles of the Au(111) modified electrodes with (a) (50:1) mixed SAM, (b) (50:1) SAM/Au-NPs, (c) (50:1) SAM/Au-NPs/$C_{10}$-SH, and (d) (50:1) SAM/Au-NPs/$C_{10}$-SH/Au-NPs, in 1 mM $K_3Fe(CN)_6$ in 0.1 M $KNO_3$ solution; $\nu = 50$ mV s$^{-1}$.

nanoparticles.[25,26] On the other hand, Yang et al. observed that upon immobilization of citrate/Au-NPs on 1,6-hexanedithiol and 1,9-nonanedithiol SAMs, in $K_3Fe(CN)_6$ containing solution, the ET has not been enhanced.[15] These authors suggest that, due to the repulsive interactions between negatively charged citrate/Au-NPs, only a submonolayer of nanoparticles can be immobilized on the dithiol SAMs, which has been considered the reason for the observed poor reversibility for the $Fe(CN)_6^{3-/4-}$ redox probe. However, since a less organized $C_{10}$-SH than the mixed (50:1) SAM is formed, the origin of the improved ET detected for the former modified electrode upon Au-NPs immobilization, Figure 8, may be 2-fold: due to electron transfer occurring at defect and collapsed sites within the monolayer and due to the presence of Au-NPs.

The formation of a $C_{10}$-SH monolayer on the nanoparticles surface only partially blocked the ET and the voltammetric profile of the base SAM modified electrode (first layer) has not been restored (possibly due to an imperfect SAM adsorbed on the Au-NPs surface) revealing the contribution from the underlying Au-NPs layer, as illustrated in Figure 8. For the exposed second Au-NPs layer, the reversibility of the redox process has been improved and a significant increase in the electrochemical response was observed in the cyclic voltammograms shown in Figure 8. In fact, a similar effect, in 1,6-hexanedithiol and citrate/Au-NPs multilayers, has been observed by Lu et al.; for the exposed Au-NPs layer, the electrochemical behavior changed from resistive ($n < 3$ layers) to sigmoidal ($n = 3$) and to a linear diffusion profile with $n > 3$ as the number of layers increased.[25]

From the electrochemical data presented earlier it was concluded that the (50:1) mixed SAMs are more organized than those prepared from pure dithiol solutions; this more ordered SAM may prevent the ET occurring predominantly at defect and collapsed sites and thus higher contribution from the Au-NPs is expected in the overall electrochemical response.

In fact, a less reversible redox process has been observed for the mixed SAM/Au-NPs than for the dithiol/Au-NPs modified electrode, probably due to better blocking effect of the SAM layer. However, at potential values lower than ca. −50 mV, higher reduction current was detected in the mixed SAM/Au-NPs modified electrode, as illustrated in Figure 9. The formation of a $C_{10}$-SH SAM on the Au-NPs surface significantly changed the voltammetric profile; a reversible ($\Delta Ep = 75$ mV) peak shaped voltammogram was obtained and the electrochemical response at potential values below ~100 mV (reduction) and above ~250 mV (oxidation) has been blocked, confirming that the Au-NPs surface was modified by the $C_{10}$-SH SAM. The formation of a second Au-NPs layer increased the ET, higher redox current and reversible behavior were detected in the cyclic voltammogram presented in Figure 9.

It is noteworthy to bring up that further investigation concerning the occurrence of more than one oxidation process in the anodic scan is still needed and will be considered in a future paper.

## Conclusions

The increasing content of 1-decanethiol in the preparation solution of mixed (1-decanethiol:1,10-decanedithiol) SAMs enhanced its stability and organization. Support for this conclusion was obtained from the negative shift of the reductive desorption potential and increase of surface coverage by increasing the thiol concentration. Electron transfer data indicate increasing ET hindrance in the order (50:1) > (10:1) ≈ (5:1) > $C_{10}$-SH SAM, which further supports that more stable and organized SAMs were obtained with an increase in 1-decanethiol.

The attachment of a submonolayer of citrate-stabilized Au-NPs, of spherical shape with average diameter of about 15 nm, and a tendency to display the surface slightly dominated by the (111) facets, to either pure dithiol or mixed (50:1) SAMs, monitored by EQCM showed that different quantities of Au-NPs can be immobilized on the modified surface by controlling the adsorption time, composition of SAM, through the amount of −SH groups at the SAM/solution interface, and the adequate positioning of the free functional groups.

As the layer-by-layer SAM/Au-NPs architectures were developed, the surface morphology evolution has been characterized by AFM. Upon Au-NPs immobilization on the $C_{10}$-SH

SAM, the smooth SAM surface became rougher and spherical features with diameter comparable to that of the Au-NPs were detected; the phase image clearly showed the attachment of the nanoparticles to the SAM by increased phase contrast due to distinct viscoelastic properties of the organic layer and the Au-NPs. The formation of a new dithiol monolayer was confirmed by the reappearance of a homogeneous and smoother layer.

Although a submonolayer of Au-NPs was attached to both pure $C_{10}$-SH and mixed (50:1) modified electrodes (a similar behavior was expected for the successive Au-NPs layers) and disorganized $C_{10}$-SH SAMs were formed on the Au-NPs surface, the presence of these metallic islands enhanced ET at each nanoparticle layer level. The higher ordered mixed SAM than that of the pure dithiol SAM seems to enable distinguishing the contribution of the Au-NPs from that of collapsed and defect sites in the SAM for the electrochemical response.

**Acknowledgment.** V.C.F. grateful acknowledges the financial support from Fundação para a Ciência e a Tecnologia, scholarship SFRH/BD/30585/2006, and Dr. Ana Viana, SPM Laboratory (CQB/FCUL), for the AFM images.

## References and Notes

(1) Love, J. C.; Estroff, L. A.; Kriebel, J. K.; Nuzzo, R. G.; Whitesides, G. M. *Chem. Rev.* **2005**, *105*, 1103.
(2) Ulman, A. *Chem. Rev.* **1996**, *96*, 1533.
(3) Jiang, W.; Zhitenev, N.; Bao, Z.; Meng, H.; Abusch-Magder, D.; Tennant, D.; Garfunkel, E. *Langmuir* **2005**, *21*, 8751.
(4) Kohale, S.; Molina, S. M.; Weeks, B. L.; Khare, R.; Hope-Weeks, L. J. *Langmuir* **2007**, *23*, 1258.
(5) Ferreira, V. C.; Silva, F.; Abrantes, L. M. *Chem. Biochem. Eng. Q.* **2009**, *23*, 99.
(6) Kohli, P.; Taylor, K. K.; Harris, J. J.; Blanchard, G. J. *J. Am. Chem. Soc.* **1998**, *120*, 11962.
(7) Joo, S. W.; Han, S. W.; Kim, K. *Langmuir* **2000**, *16*, 5391.
(8) Joo, S. W.; Han, S. W.; Kim, K. *J. Phys. Chem. B* **2000**, *104*, 6218.
(9) Esplandiu, M. J.; Hagenstrom, H. *Solid State Ionics* **2002**, *150*, 39.
(10) Carot, M. L.; Esplandiu, M. J.; Cometto, F. P.; Patrito, E. M.; Macagno, V. A. *J. Electroanal. Chem.* **2005**, *579*, 13.
(11) Esplandiu, M. J.; Carot, M. L.; Cometto, F. P.; Macagno, V. A.; Patrito, E. M. *Surf. Sci.* **2006**, *600*, 155.
(12) Liang, J.; Rosa, L. G.; Scoles, G. *J. Phys. Chem. C* **2007**, *111*, 17275.
(13) Garcia-Raya, D.; Madueno, R.; Sevilla, J. M.; Blázquez, M.; Pineda, T. *Electrochim. Acta* **2008**, *53*, 8026.
(14) Leung, T. Y. B.; Gerstenberg, M. C.; Lavrich, D. J.; Scoles, G. *Langmuir* **2000**, *16*, 549.
(15) Yang, M.; Zhang, Z. *Electrochim. Acta* **2004**, *49*, 5089.
(16) Bethel, D.; Brust, M.; Schiffrin, D. J.; Kiely, C. *J. Electroanal. Chem.* **1996**, *409*, 137.
(17) Stolaczyk, K.; Bilewicz, R. *Electrochim. Acta* **2006**, *51*, 2358.
(18) Chirea, M.; Cruz, A.; Pereira, C. M.; Silva, A. F. *J. Phys. Chem. C* **2009**, *113*, 13077.
(19) Brust, M.; Blass, P. M.; Bard, A. J. *Langmuir* **1997**, *13*, 5602.
(20) Deng, W.; Yang, L.; Fujita, D.; Nejoh, H.; Bai, C. *Appl. Phys. A: Mater. Sci. Process.* **2000**, *71*, 639.
(21) Qu, D.; Uosaki, K. *J. Phys. Chem. B* **2006**, *110*, 17570.
(22) Ohgi, T.; Sheng, H.-Y.; Dong, Z.-C.; Nejoh, H.; Fujita, D. *Appl. Phys. Lett.* **2001**, *79*, 2453.
(23) Ohgi, T.; Sheng, H.-Y.; Nejoh, H. *Appl. Surf. Sci.* **1998**, *130*, 919–132.
(24) Boer, B.; Frank, M. M.; Jiang, W.; Garfunkel, E.; Bao, Z. *Langmuir* **2004**, *20*, 1539.
(25) Lu, M.; Li, X. H.; Yu, B. Z.; Li, H. L. *J. Colloid Interface Sci.* **2002**, *248*, 376.
(26) Su, L.; Mao, L. *Talanta* **2006**, *70*, 68.
(27) Aliganga, A. K.; Duwez, A.-S.; Mittler, S. *Org. Electron.* **2006**, *7*, 337.
(28) Walczak, M. M.; Alves, C. A.; Lamp, B. D.; Porter, M. D. *J. Electroanal. Chem.* **1995**, *396*, 103.
(29) Zhong, C.-J.; Porter, M. D. *J. Electroanal. Chem.* **1997**, *425*, 147.
(30) Zhong, C. J.; Zheng, W. X.; Liebowitz, F. L. *Electrochem. Commun.* **1999**, *1*, 72.
(31) Su, B.; Girault, H. H. *J. Phys. Chem. B* **2005**, *109*, 23925.
(32) Brust, M.; Bethell, D.; Kiely, C. J.; Schiffrin, D. J. *Langmuir* **1998**, *14*, 5425.
(33) Joseph, I.; Besnard, I.; Rosenberger, M.; Guse, B.; Nothofer, H.-G.; Wessels, J. M.; Wild, U.; Knop-Gericke, A.; Su, D.; Schlogl, R.; Yasuda, A.; Vossmeyer, T. *J. Phys. Chem. B* **2003**, *107*, 7406.
(34) Diao, P.; Jiang, D.; Cui, X.; Gu, D.; Tong, R.; Zhong, B. *J. Electroanal. Chem.* **1999**, *464*, 61.
(35) Turkevich, J.; Stevenson, P. C.; Hiller, J. *Discuss. Faraday Soc.* **1951**, *11*, 55.
(36) Kimling, J.; Maier, M.; Okenve, B.; Kotaidis, V.; Ballot, H.; Plech, A. *J. Phys. Chem. B* **2006**, *110*, 15700.
(37) Link, S.; El-Sayed, M. A. *J. Phys. Chem. B* **1999**, *103*, 4212.
(38) Jana, N. R.; Gearheart, L.; Murphy, C. J. *Langmuir* **2001**, *17*, 6782.
(39) Chen, H.; Kou, X.; Yang, Z.; Ni, W.; Wang, J. *Langmuir* **2008**, *24*, 5233.
(40) Widrig, C. A.; Alves, C. A.; Porter, M. D. *J. Am. Chem. Soc.* **1991**, *113*, 2805.
(41) Phong, P. H.; Sokolov, V. V.; Nishi, N.; Yamamoto, M.; Kakiuchi, T. *J. Electroanal. Chem.* **2007**, *600*, 35.
(42) Bruckenstein, S.; Shay, M. *Electrochim. Acta* **1985**, *30*, 1295.

JP912123M